ISBN: 978-3-95450-253-0 ISSN: 2673-5571 doi:10.18429/JACoW-HB2023-WEC1I1

RADIATION HARDENED BEAM INSTRUMENTATIONS FOR MULTI-MEGA-WATT BEAM FACILITIES

K. Yonehara*, Fermilab, Batavia, IL, USA

Abstract

Beam instrumentation is a critical component for the successful operation of particle accelerators, integrating beam diagnostics and beam control systems into beam optics. However, the performance of beam instrumentation is often constrained by factors such as prompt radiation dose, integrated radiation dose, operational (ambient) temperature and humidity, available space, and the strength of embedded electromagnetic fields at the monitoring point. These constraints can limit the dynamic range of operational beam parameters, including the maximum achievable beam power. To address this, a seamless R&D effort should be dedicated to developing radiation-hardened beam instrumentation for future multi-Mega-Watt beam facilities. In this paper, we describe a radiation-hardened beam instrumentation system based on the operational experience gained from the NuMI beam line.

INTRODUCTION

Modern beam facilities employ advanced accelerator technology to generate intense beams for exploration across a wide range of accelerator applications, such as a collider, accelerator neutrino beam, intense muon source, spallation neutron source, accelerator-driven subcritical nuclear reactor, Radioactive-Isotope (RI) beam, etc. Table 1 shows the beam parameter of a selected beam facilities [1, 2].

Each facility faces the challenge of developing radiation-hardened beam instrumentation which is operated in severe environments. Some examples are provided in Ref. [1]. In this paper, we specially address the challenge of radiation-hardened beam instrumentation, drawing on our experience with the operation of NuMI targetry system, especially in the context of a future accelerator neutrino facility.

Beam instrumentation plays an essential role in ensuring the successful operation of particle accelerators. Its primary function is to characterize the beam phase space by measuring various parameters related to an ensemble of charged particles. These parameters include:

- Spatial distribution: this determines the spatial characteristics of the charged particle ensemble, including the centroid position, orientation, and profile of the beam ensemble.
- Intensity measurement: this involves quantifying the amount of beam ensemble in a certain time period.
- Time structure measurement: this includes assessing the time differential beam intensity and the bunch structure of the charged particle ensemble.

The beam instrumentation often incorporates a feedback loop to maintain stable beam operation. The concept of a feedback loop system differs between circular and linear accelerators.

In a circular accelerator, where the beam circulates for many revolutions, the beam parameters of the same beam ensemble can be adjusted via a feedback loop system. On the other hand, in a linear accelerator, the beam parameters cannot be corrected for the same beam ensemble because the beam passes through the accelerator only once. Therefore, a feedback loop system is applied to correct the beam parameters for the next incoming beam ensemble.

Additionally, the beam instrumentation serves as an anomaly detector. If the observed parameter exceeds some threshold, the feedback loop triggers a special signal to the beam control system. In the worst case, the beam control system aborts the beam to protect the accelerator or maintain beam quality.

In the case of NuMI targetry system operation, special beam instrumentation is used to monitor and control the proton beam in the transport line reaching the target. We demonstrate the beam control system and the beam abort signal in the NuMI targetry system in the beam control and beam permit systems section.

Especially, the thermocouple beam position sensor positioned in front of the target is an extremely reliable detector, even when intercepting the intense proton beam. We present the performance of the thermocouple beam position sensor in the thermocouple beam position monitor section.

The neutrino target is usually bare, or minimize the use of supporting structure materials for the target. Materials surrounding the target that do not contribute pion production, could absorb pions originally created at the target. Consequently, there is no in-situ target health monitor for the neutrino target. In the NuMI targetry system, four layers of ionization chamber grid downstream of the target and horns are used to monitor the condition of the targetry system. We present the performance of the ionization chambers in the following section. The first ionization chamber, referred to as the hadron monitor, was inspected after the beam operations, revealing various types of the radiation damage. We present those damages in the hadron monitor section.

BEAM INSTRUMENTATION IN NuMI

Figure 1 depicts the layout of the NuMI target and horn system (referred to as "targetry system"), including the four layers of ionization chamber grids. Every 1.2 s, a 120 GeV proton beam is transported from the Main Injector to the NuMI target system. The beam spill length is 9.6 ms. The highest beam intensity is 5.6×10^{13} protons on target (POT) per spill demonstrated in Spring 2022. The proton beam

* yonehara@fnal.gov

ISBN: 978-3-95450-253-0 ISSN: 2673-5571 doi:10.18429/JACoW-HB2023-WEC1I1

Table 1: Beam parameters reported in the radiation hardened beam instrumentation workshop [3]. Values in parenthesis indicate future plans.

Institution	Beam Energy [GeV]	Beam Intensity	Beam Power	Radiation Dose
CERN CNGS	400	2.4×10^{13} protons per pulse	500 kW	$<1 \times 10^{9}$ mSv/h [4]
CERN LHC (Run 3)	1,800	$1.8 \times 10^{11} \times 2748$ protons per beam	362 MJ per beam	
Fermilab NuMI	120	$5.5\ (6.5) \times 10^{13}$ protons per 1.2 s	870 kW (1 MW)	1×10^{10} mSv/h
Fermilab LBNF	60—120	7.5×10^{13} protons per 0.7 s to 1.2 s	1.2 MW to 2.4 MW	$<1 \times 10^{12}$ mSv/h
J-PARC neutrino	30	3.2×10^{14} protons per 2.48 s (1.32 s)	515 kW (700 kW)	
J-PARC MLF	3	4.5×10^{8} protons per pulse, 25 Hz	730 kW (1 MW)	30 MGy/6y
ESS	2	8.9×10^{14} protons per pulse, 14 Hz	5 MW	$<1 \times 10^{9}$ mSv/h [5]
SNS	1 (1.3)	1.5×10^{14} protons per beam	1.4 MW (2 MW)	as high as 1×10^{12} Rad

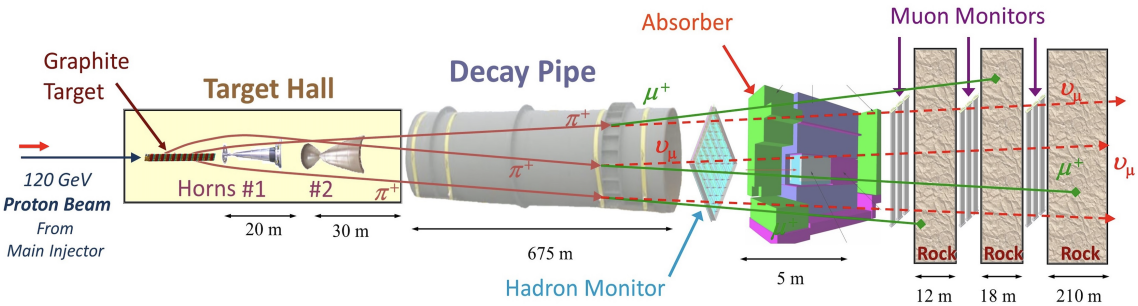

Figure 1: The overall layout of the NuMI beamline.

Table 2: NuMI Beam Instrumentation and its Accuracy

Beam parameter	Design value	Tolerance	Beam instr.	Accuracy
Horn current	200 kA	±2 kA	Horn CT	0.1 %
Horiz. beam position on target	0 mm	±1 mm	BPM, TC	0.02 mm
Vertical beam position on target	0 mm	±1 mm	BPM, TC	0.02 mm
RMS beam spot size	1.3 mm	±0.2 mm	Beam PM	0.1 mm
Beam intensity	50×10^{12} POT	1 %	Beam CT	0.5 %

structure in the Main Injector and the NuMI proton beam transport line optics are described in Ref. [6].

The primary beam instrumentation and the muon monitors for the NuMI beam line are described in this section [7]. Table 2 shows a summary of the NuMI proton beam instrumentation and the horn current monitor.

Proton Beam Monitor

A pair of induced-charge pickup electrodes and a multi-wire Secondary Emission electron Monitor (SEM) are used as a beam position monitor (BPM) and beam profile monitor (PM), respectively. A special PM, which is permanently placed upstream of the target, is made of a thin (5 μm thick × 25 μm wide) Ti foil to mitigate beam scattering. There are 47 × 47 foils stretched in both x and y, with 0.5 mm gap in between. The PM provides the proton beam profile for every spill. Other PMs are periodically inserted in the beam line at different locations for monitoring the beam optics. Horizontal and vertical BPMs are paired to measure the beam position on the transverse plane. Two sets of paired BPMs near the target are used for measuring the proton beam position and beam orientation at the target. Several BPMs comprise a network system to automatically correct the proton beam position and beam orientation at the target, which is called the autotune. The accuracy of the beam position measurement is ±0.02 mm using BPM and PM, and the accuracy of the RMS beam spot size measurement is ±0.1 mm using PM.

Current Monitor

The proton beam intensity at the target is measured by using a toroidal beam Current Transformer (beam CT) located upstream of the target. The signal calibration is done by using a current source and by comparison to a Direct-Current Current Transformer (DCCT) at the Main Injector. The accuracy of the beam CT is 0.5 % while the stability of signal pulse-per-pulse is ± 0.1 %.

The horn power supply circuit generates a half-sinusoidal voltage, and the pulse is propagated through four striplines. The total pulse length of this half sinusoidal wave is 2.334 ms. A current transformer measures the horn current for each stripline (horn CT). The current transformer is calibrated

ISBN: 978-3-95450-253-0 ISSN: 2673-5571 doi:10.18429/JACoW-HB2023-WEC1I1

using a pre-calibrated current source. The accuracy of horn CT is ±0.1 %.

Feedback Loop and Beam Permit Systems in the NuMI Proton Beam Transport Line

The feedback loop for beam control involving trim magnets in the NuMI beam transport line is established by the BPM signals along the beam line. The program controlling the feedback loop is referred as "autotune" [6]. Because the transport line operates as a single pass, the feedback is applied for the next incoming beam. As a result, the RMS beam position and beam orientation at the target remains within ±0.2 mm and ±28 μrad, respectively, during annual beam operations by using autotune.

The beam permit system oversees beam loss, temperature change of specific components, and variation of beam parameters. There are a total of 48 sealed gas ionization chambers along the NuMI beam line to monitor beam loss. The threshold of the beam loss rate is set at 0.002 rad/s. If the measurement exceeds this threshold value, the beam is halted. Several temperatures of the critical devices are also recorded in the beam permit system. Here, we examine a critical device which is significantly impacted by the beam power upgrade. A 1.5 m-long baffle in front of the target protects the target, horn necks, and absorber from the mis-steered beam. Three thermocouple sensors are used to measure the baffle temperature and to trigger the beam permit for stopping the mis-steered beam. There are two critical beam windows and their temperatures are recorded in the beam permit system. The beam window at the end of the proton beam line serves as the critical interface between high vacuum and air conditions. Another critical beam window is located downstream of the target canister. Due to the wide scattering of the beam at the target, the beam can hit the welded part of the window. The temperature increase of the window flange is carefully monitored during the beam operations. The BPM in the NuMI beam line has a threshold, triggering the beam permit if the measurement exceeds it. We also apply the threshold on the beam intensity monitor.

Thermocouple Beam Position Sensor

There is a 1.5 mm-diameter beryllium rod in front of the NuMI target (shown in Fig. 2). Two sets of three Be rods are stretched in the transverse plane to intercept the beam. Each set is directed in horizontal and vertical directions. The gap between the axial centres of the rods is 1.3 mm which corresponds to the expected RMS beam spot size at the target. In this configuration, the beam position measurement is the most sensitive. One end of each rod is attached to a heat sink, while the other end is connected to a thermocouple sensor. As the proton beam delivered into the target deposits its kinetic energy, the rod's temperature increases. The thermocouple sensor detects this temperature increment. Remarkably, the thermocouple sensor survives under 1×10^{10} mSv/h radioactive environments for several years. The sensor calibration with a known beam intensity needs to be done frequently since the temperature value from the thermocouple sensor is not reliable after the beam irradiation.

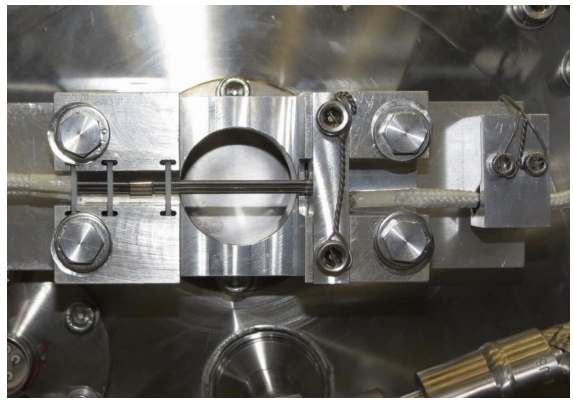

Figure 2: Vertical thermocouple sensor.

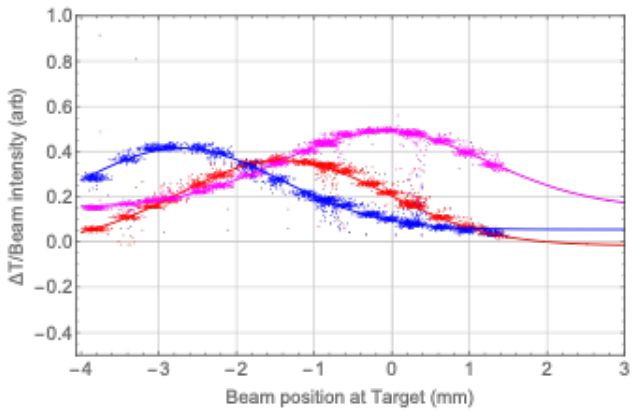

Figure 3: Observed vertical beam scan by using the thermocouple sensor. A red point is the observed temperature at the centre rod (f_1), a magenta and blue points are the observed temperate at the top (f_2) and bottom (f_3) rods, respectively.

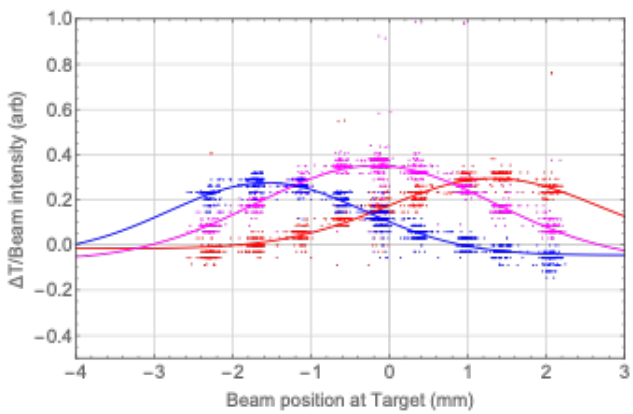

Figure 4: Observed horizontal beam scan by using the thermocouple sensor. A magenta point is the observed temperature at the centre rod (g_1), red and blue points are the observed temperature at the right (g_2) and left (g_3) rods with respect to the beam direction, respectively.

Figures 3 and 4 show the calibration run of the thermocouple sensor which was taken in 2018. The beam intensity

ISBN: 978-3-95450-253-0 ISSN: 2673-5571 doi:10.18429/JACoW-HB2023-WEC1I1

was fixed around 2.0×10^{13} particles per beam spill. A solid curve represents a Gaussian fit with an offset. We obtain three calibration curves. The estimated peak position from the fitting indicates the centre axis position of the rod, and the gap between peaks is the axis position gap of the rod. The resolution of horizontal beam scan is worse than the vertical one since the coarser ADC is used for the horizontal measurement.

Figures 5 and 6 show the estimated vertical and horizontal beam positions at the target from the thermocouple sensor, respectively. A blue solid line represents the temperature ratio delivered from two calibration curves, where f_1 and g_1 correspond to the calibration curves from the centre rod in each direction. A red point represents the target centre, while a bold red line shows the position range between -0.2 and 0.2 mm, and a thinner red line represents the position range between -0.5 and 0.5 mm. A primary source of deviation from the solid line is due to fluctuations in beam intensity.

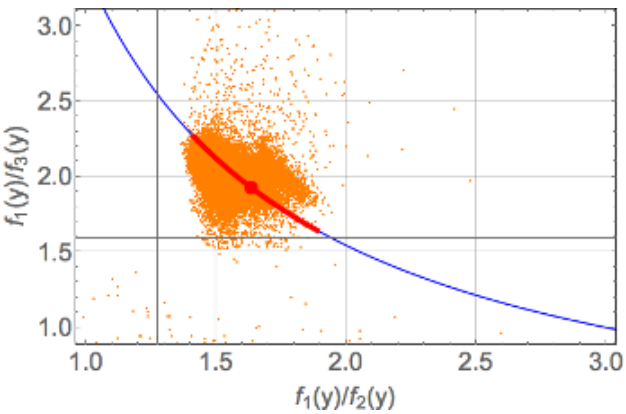

Figure 5: Estimated vertical proton beam position at the target from the thermocouple sensor.

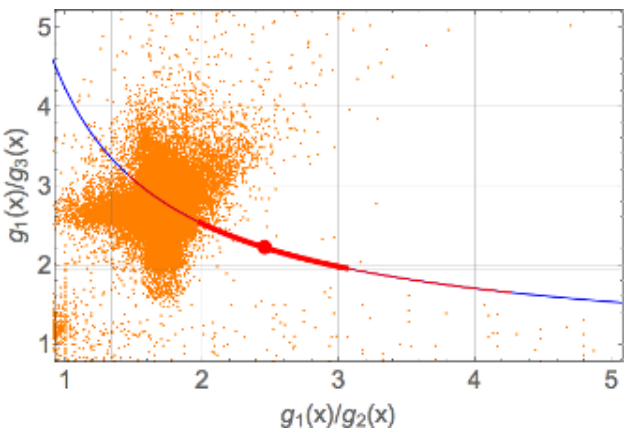

Figure 6: Estimated horizontal proton beam position at the target from the thermocouple sensor.

Another major systematics in the thermocouple sensor measurement is the time constant. Figure 7 shows the observed temperature from one of thermocouple sensors. A blue and orange points are the raw value. Because the NuMI beam time sequence occasionally involves a supercycle in which the beam is delivered into the fixed target beam line every minute. There is a 6 s gap during the supercycle which is sufficiently long to cool the beryllium rod. Given that time constant of the thermocouple sensor is approximately a minute, the temperature observed by the sensor does not reach the equilibrium during the supercycle. We select data points which is close to the equilibrium temperature to estimate the beam position. It suggests that the thermocouple beam position sensor needs a calibration run whenever the beam intensity is changed.

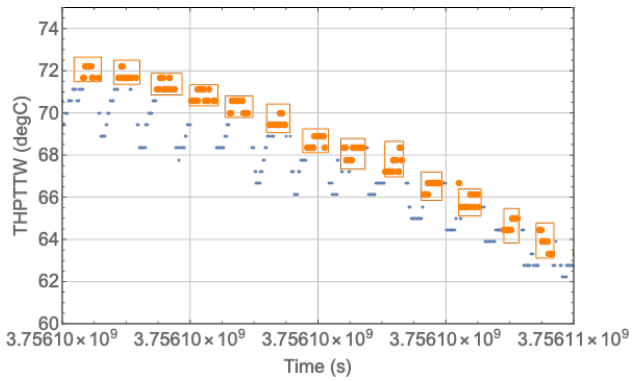

Figure 7: The observed raw temperature value from the thermocouple sensor during the supercycle. An orange box is the analysis gate to select data for estimating the beam position at the target from the thermocouple sensor.

Hadron Monitor

The first layer of ionization chamber, referred to as the hadron monitor, is located at the downstream end of the decay pipe. It consists of a 5 × 5 grid of ionization chambers. Pure helium gas is used as the ionization material. The hadron monitor serves primarily for proton beam-based alignment [7]. Positions of the target and horns are determined through proton beam tomography. The accuracy of the beam-based alignment is typically within ± 0.1 mm, consistent with optical survey results performed whenever a beam element is installed or replaced.

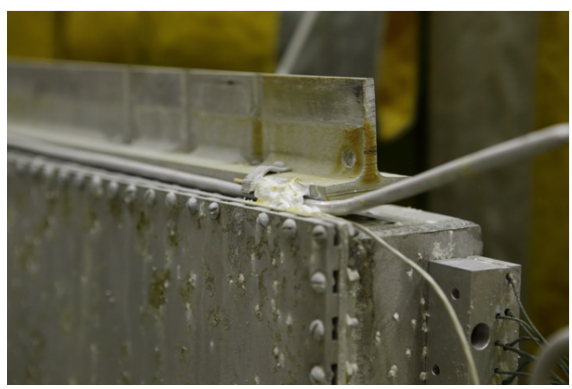

Figure 8: Picture shows the upper right of the hadron monitor which used in the NuMI beamline for a couple of years.

The hadron monitor is directly exposed to radiation from the target. The estimated radiation dose at the hadron monitor is $\sim 1 \times 10^5$ mSv/h. Because of such a high radiation

ISBN: 978-3-95450-253-0 ISSN: 2673-5571 doi:10.18429/JACoW-HB2023-WEC1I1

exposure, the hadron monitor has sustained significant radiation damage. Figure 8 shows the hadron monitor which had been operated in the NuMI beam line for a couple of years. The radiation induces chemical changes in the ambient gas, leading to the formation of highly reactive chemical species. As a result, the surface material of the hadron monitor, which is aluminium, has undergone rusting.

Muon Monitors

Figure 9 shows a schematic drawing of the muon monitor. Each muon monitor consists of a 9 × 9 grid of ionization chambers. Each chamber has a 7.5 × 7.5 cm^2 sensing area

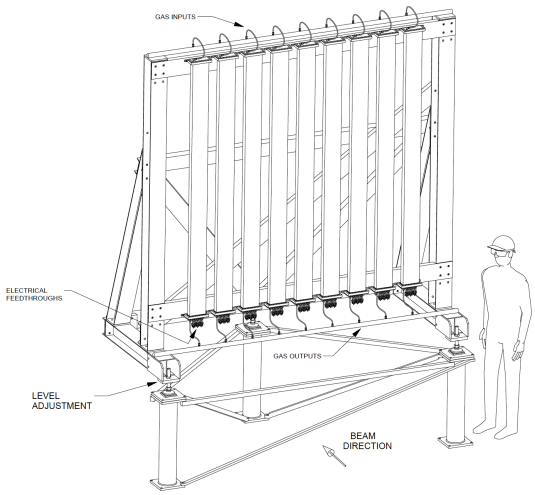

Figure 9: Muon monitor engineering drawing showing the nine tubes containing a row of nine pixels each.

with Ag-Pt plated electrode on a 1 mm-thick Alumina ceramic electrode base, and the gap between the electrodes is 3 mm. The distance between the centres of channels is 250 mm to cover a 2.1 × 2.1 m^2 area. Nine ionization chambers are installed in a rectangular aluminium tube. There are nine tubes assembled vertically on a support structure in the beam line. Atmospheric-pressure 99.999 % pure Helium gas is used as an ionization media, injected from the top and exhausted from the bottom of each tube. The bias voltage is 300 V in which the ionization chamber is on the plateau where all ionized charged particles in the chamber are collected at the electrodes without charge multiplication [7].

Figures 10–12 show an example of the observed pixel image per spill. The pedestal signal, taken when the beam is turned off, is subtracted from the beam-on signal. The signal for each channel was calibrated using a radiation source before the monitor was installed in the beam line. The integrated signal from all channels is normalized by the beam intensity per beam spill and is monitored during beam operation. The long-term fluctuation of the integrated signal normalized by the beam intensity is ±0.2 % for Muon Monitors 1 and 2 while the fluctuation of normalized Muon Monitor 3 signal is slightly higher at ±0.5 %. It is found that the observed pixel image pattern is not changed by the beam intensity although the signal size is proportional to the beam intensity.

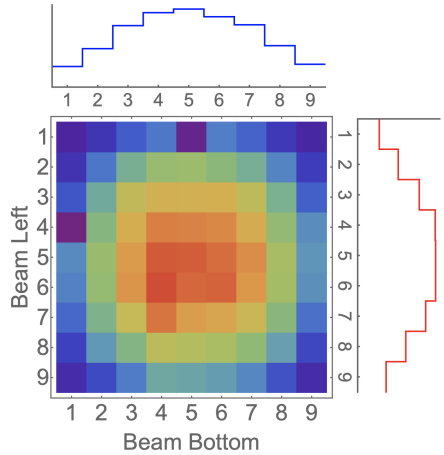

Figure 10: The observed beam profile at Muon Monitor 1. The top and right subplots show the projection of the beam profile in horizontal and vertical planes, respectively. The scale on top and right plots is linear.

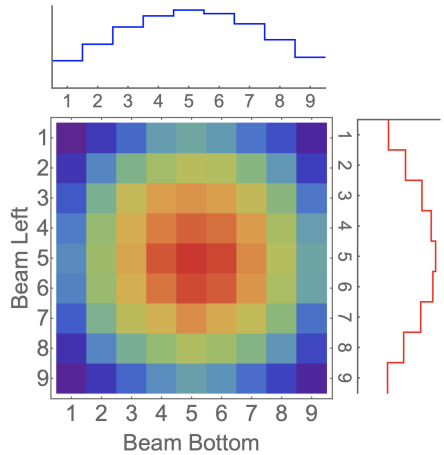

Figure 11: The observed beam profile at Muon Monitor 2. The top and right subplots show the projection of the beam profile in horizontal and vertical planes, respectively. The scale on top and right plots is linear.

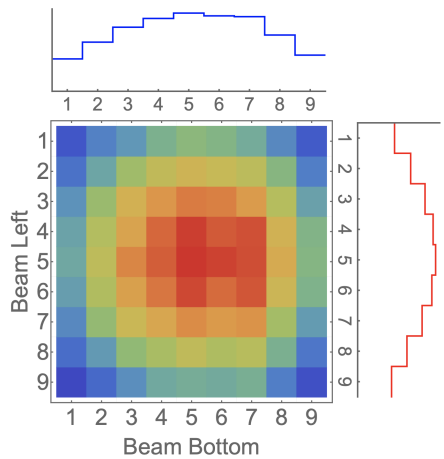

Figure 12: The observed beam profile at Muon Monitor 3. The top and right subplots show the projection of the beam profile in horizontal and vertical planes, respectively. The scale on top and right plots is linear.

ISBN: 978-3-95450-253-0 ISSN: 2673-5571 doi:10.18429/JACoW-HB2023-WEC1I1

The muon monitors are located downstream of the hadron absorber and separated by 12 and 18 m of rock (see Fig. 1). The muons reaching the monitors lose part of their kinetic energy in the material via energy loss processes. Therefore, the initial spectrum of muons when they are produced differs from the spectrum at the monitors. Figure 13 suggests that each monitor detects a different muon phase space with a specific cut-off energy.

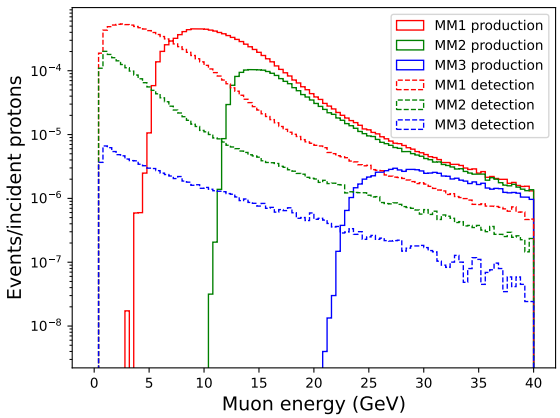

Figure 13: Simulated muon spectra. A solid red line represents the muon spectrum when muons are produced while a dashed red line is the muon spectrum at Muon Monitor 1. The shift is because muons have lost energy in the absorber. The green and blue lines are for Muon Monitor 2 and 3, respectively.

Future Study of Muon Monitor as Monitoring Targetry System

It is established that the parabolic-shaped magnetic horn is a linear beam optics [8]. The validation is supported by experimental study on the magnetic horn focusing mechanism study [7]. We also found that the magnetic horn has a strong chromaticity. It suggests that the muon monitor image contains not only the cross section of transverse phase space of muons at the monitor position, but also the initial kinetic energy of pions. A preliminary simulation study was made to determine the strength of horn chromaticity. Consequently, each channel of the monitor is assigned a specific muon spectrum. We are in the process of preparing Time of Flight (ToF) measurements at each channel of the monitor to validate the simulation study.

ACKNOWLEDGEMENTS

We would like to thank the Fermilab Accelerator Operations, Target Systems, External Beam Delivery, and Main Injector Departments for their contributions to this study. We also want to thank the NOvA collaboration for providing us with an opportunity to run the special beam tests.

This work is supported by the Fermi Research Alliance, LLC manages and operates the Fermi National Accelerator Laboratory pursuant to Contract number DE-AC02-07CH11359 with the United States Department of Energy.

This work is partially supported by the U.S. Department of Energy grant DE-SC0019264.

REFERENCES

[1] K. Yonehara, "Radiation hardened beam instrumentations for multi-Mega-Watt beam facilities", Mar. 2022, unpublished. doi:10.48550/arXiv.2203.06024

[2] F. Pellemoine *et al.*, "High-power targetry R&D and support for future generation accelerator", *J. Instrum.*, vol. 18, p. T07006, 2023. doi:10.1088/1748-0221/18/07/T07006

[3] "Radiation-hardened beam instrumentation workshop", unpublished. https://indico.fnal.gov/event/52543/

[4] M. Lorenzo *et al.*, "Computational and Analytical Estimation of the Prompt Dose Equivalent Rate in the CNGS Installation", CERN-OPEN-2006-009. https://cds.cern.ch/record/924395

[5] A. Alekou *et al.*, "The European Spallation Source neutrino Super Beam", Mar. 2022, unpublished. doi:10.48550/arXiv.2203.08803

[6] P. Adamson *et al.*, "The NuMI Neutrino Beam", *Nucl. Instrum. Methods Phys. Res. Sect. A*, vol. 806, p. 279, 2016. doi:10.1016/j.nima.2015.08.063

[7] K. Yonehara *et al.*, "Exploring the focusing mechanism of the NuMI horn magnets". doi:10.48550/arXiv.2305.08695

[8] S. Kopp, "Accelerator Neutrino Beams", *Phys. Reports*, vol. 439, pp. 101–159, 2007. doi:10.1016/j.physrep.2006.11.004